2017

Multi-Rate LQR Control of a Multi-Machine MVDC Shipboard Electric Distribution System with Constant Power Loads

Mills, Adam J.; Ashton, Robert W.

Multi-Rate LQR Control of a Multi-Machine MVDC Shipboard Electric Distribution System with Constant Power Loads

Lieutenant Commander Adam J. Mills, USN
Department of Electrical and Computer Engineering
Naval Postgraduate School
Monterey, CA, USA
ajmills@nps.edu

Robert W. Ashton, Ph.D
Department of Electrical and Computer Engineering
Naval Postgraduate School
Monterey, CA, USA
ashton@nps.edu

Abstract— **The future all-electric warship is expected to utilize medium-voltage DC (MVDC) main distribution to supply several load zones. The load zones will convert the MVDC power to lower voltage for use by local loads as well as contain local energy storage for casualty back-up power. A majority, if not totality, of loads are expected to exhibit constant-power load (CPL) behavior. While many papers have developed single-input control schemes to regulate MVDC bus voltage where CPLs are present, multi-input controller schemes have not been explored. This paper presents two implementations of adaptive, multi-rate LQR controllers to regulate system voltages during step load transients. Through coordinated use of switching converter based low-rate DC voltage sources and high-rate energy storage device currents, multi-rate LQR controllers can provide excellent bus regulation by leveraging of all available control input devices. A periodic discrete-time multi-rate LQR controller (LQR-P) is described and compared to a selective-feedback, multi-rate LQR controller (LQR-SM). Both are designed and implemented in MATLAB software using a hypothetical multi-machine, multi-zone shipboard MVDC electric distribution system with CPLs and energy storage devices.**

Keywords— MVDC, constant power load (CPL), hybrid energy storage system (HESS), linear quadratic regulator (LQR), adaptive, non-linear, all-electric ships.

I. Introduction

Demand for electrical power on naval vessels is growing at an increasing rate. To meet electrical power demands while maintaining relatively small size, naval designers are exploring integrated propulsion system (IPS) concepts. While the US Navy's first IPS warship, USS Zumwalt (DD-1000), has a medium voltage AC distribution system, future concepts are focused towards medium voltage DC zonal distribution due to the many advantages of DC distribution [1]. An MVDC distribution system will require power electronics based power conversion between power generating modules (PGMs), zonal distribution and power conversion modules (PCMs) and point-of-load converters [2]. The prevalence of power conversion throughout the generation, distribution, and point of load applications implies that a majority, if not a totality, of loading may exhibit constant power load behavior.

Constant power loads (CPLs) are generated when power electronics are coupled to high-bandwidth controls to strictly regulate power quality. The geneses of CPLs, as well as the destabilizing effects of their negative non-linear impedance are well documented in [3] and [4].

A great many papers have been written describing control and stabilization methods to address CPLs. The methods developed are almost exclusively single-input control techniques. For single source systems, passive stabilization was discussed in [3] while linear PID controllers were mentioned in [4]-[7] and adaptive linear control was discussed in [8]. For control of multi-machine systems with constant power loads, a centralized control state-feedback linearization (LSF) control method was explored in [9] and [10], an adaptive backstepping method was detailed in [11], while a decentralized linear quadratic Gaussian (LQG) controller was described in [12]. Each of the methods described in [9]-[12] simplify the multi-machine system into a 2^{nd} order differential equation with single input control. Such simplifications limit control options by limiting control input to a single device or set of devices which may be simplified into a single device.

This paper presents two implementations of an adaptive multi-rate linear quadratic regulator (LQR). The presented control schemes will demonstrate a true multi-input control method, capable of seamlessly coordinating both voltage source and current source inputs of low and high bandwidth to successfully stabilize a hypothetical MVDC shipboard electric distribution system with multiple CPLs during a large instantaneous step in constant-power load. The first implementation presented models the multi-rate system as a periodic discrete time system, called here LQR-P. The second implementation uses selective LQR input-cost matrices to achieve equivalent function; we call this LQR-SM.

II. System Model

The hypothetical MVDC shipboard distribution system consists of two power generation modules (PGM), an MVDC main bus, and two load zones. Each of the two load zones is

connected to the MVDC main bus by line cabling, an intermediate DC-DC converter input-side damper filter, and an intermediate DC-DC converter operating in continuous conduction mode. Within each zone are a Hybrid Energy Storage System (HESS) and an ideal CPL. HESSs may function as controlled current sources as described in [5] and [6].

Each of the PGMs is imagined as a prime mover driving an AC generator. Generator outputs are rectified and fed to DC-DC converters. For simulation, we use average-value models consisting of controlled voltage sources in series with equivalent resistances and inductances with parallel capacitors. Each PGM interfaces directly to a 12kV MVDC main bus. Due to the relatively high voltage of the MVDC bus, a reasonable switching frequency of 1kHz is assumed for the PGMs. One PGM is 40MW while the second is 10MW for a total of 50MW of generating capacity.

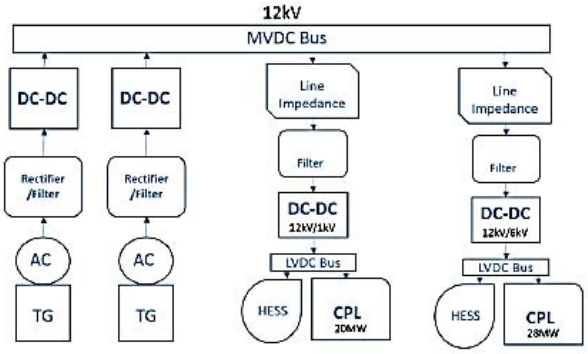

Figure 2 - Simplified Illustration of Shipboard MVDC Distribution System

To account for shipboard cabling, equivalent RLC line impedance is modeled in series with each load zone. Each load zone consists of a series damped RC filter in parallel with the medium voltage side of a power conversion module (PCM). PCMs are modeled as buck DC-DC converters operating in continuous conduction mode (CCM) at fixed duty cycles. The average value model of the DC-DC converter is a controlled current source on the medium voltage side and a controlled voltage source on the low voltage side. The power flow into the converter is held equal to the power flow out of the converter to maintain conservation of power. The equivalent average-value buck inductance and filter capacitance are modeled on the low voltage side of the converter. Since the HESSs act in relatively low voltage compared to the PGMs, they are switched with much greater speed at 8kHz. The first load zone has a 20MW CPL on a 1kV bus while the second zone has a 30MW CPL on a 6kV bus. An overview block diagram of the distribution system is shown in Fig. 2 with the circuit model shown in Fig. 3. The Fig. 3 circuit model differential equations are shown in (1).

The circuit topology does not lend itself to simplification to a 2nd order model as described in Refs. [9]-[11]. The CPLs in Fig. 3 are separated from the main bus by intermediate DC-DC converters. The load zones are not simplified into CPLs since the intermediate DC-DC converters are also operating at 12kV just like the PGM DC-DC converters, so they too would have a relatively low bandwidth. One of the conditions for CPL behavior is that the DC-DC converter acting as the load has a much greater bandwidth than the power supply. Since this is not the case, we must account for the intermediate DC-DC converter dynamics. The duty cycle of each intermediate DC-DC converter is constant, since stabilizing control will be provided by the PGMs and HESSs.

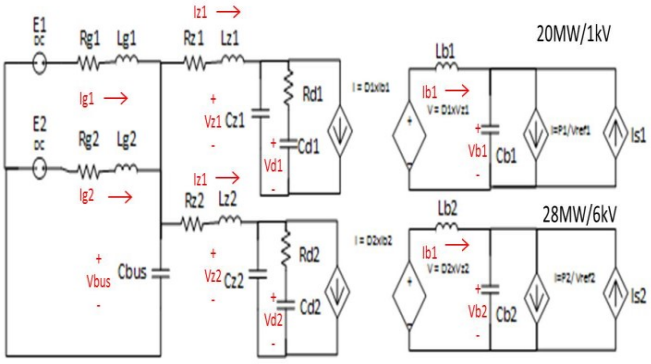

Figure 3 – Average Value Circuit Model of Shipboard MVDC Distribution System

$$
\begin{aligned}
dIg_1 &= \left(\frac{1}{Lg_1}\right) * \left(E_1 - Rg_1 * Ig_1 - V_{bus}\right) \\
dIg_2 &= \left(\frac{1}{Lg_2}\right) * \left(E_2 - Rg_2 * Ig_2 - V_{bus}\right) \\
dV_{bus} &= \left(\frac{1}{C_{bus}}\right) * \left(Ig_1 + Ig_2 + Ig_3 + Ig_4 - Iz_1 - Iz_2 - Iz_3\right) \\
dIz_1 &= \left(\frac{1}{Lz_1}\right) * \left(V_{bus} - Rz_1 * Iz_1 - Vz_1\right) \\
dIz_2 &= \left(\frac{1}{Lz_2}\right) * \left(V_{bus} - Rz_2 * Iz_2 - Vz_2\right) \\
dVz_1 &= \left(\frac{1}{Cz_1}\right) * \left(Iz_1 - Id_1 - d_1 * Ib_1\right) \\
dVz_2 &= \left(\frac{1}{Cz_2}\right) * \left(Iz_2 - Id_2 - d_2 * Ib_2\right) \\
dVd_1 &= \left(\frac{1}{Cd_1}\right) * \frac{Vz_1 - Vd_1}{Rd_1} \\
dVd_2 &= \left(\frac{1}{Cd_2}\right) * \frac{Vz_2 - Vd_2}{Rd_2} \\
dIb_1 &= \left(\frac{1}{Lb_1}\right) * \left(d_1 * Vz_1 - Vb_1\right) \\
dIb_2 &= \left(\frac{1}{Lb_2}\right) * \left(d_2 * Vz_2 - Vb_2\right) \\
dVb_1 &= \left(\frac{1}{Cb_1}\right) * \left(Ib_1 - \frac{P_1}{Vb_1} + Is_1\right) \\
dVb_2 &= \left(\frac{1}{Cb_2}\right) * \left(Ib_2 - \frac{P_2}{Vb_2} + Is_2\right)
\end{aligned}
\tag{1}
$$

where:
E_x is the PGM voltage
Ig_x is the PGM inductor current
V_{bus} is the MVDC bus voltage
Iz_x is the line current to zone 'x'
Vz_x is the voltage at the input to buck converter 'x'
Vd_x is the voltage across the damper capacitor for zone 'x'
Ib_x is the buck inductor current for zone 'x'
Vb_x is the voltage on the buck filter capacitor for zone 'x'
Is_x is the current injected from HESS 'x'
d_x is the duty cycle for the buck converter for zone 'x'

III. CONTROL SCHEME

The control schemes of Refs. [9]-[12] rely on the ability to simplify the problem into a 2nd order single-input single-output control problem. By using a linear quadratic regulator based control scheme, the simplifying assumptions can be eliminated. A multiple-input control scheme allows the combined and coordinated use of both PGMs and HESSs to improve the system transient response to step changes in load.

A. LQR Basic Description

LQR is a popular control technique that can be used on any N-dimensional system of 1st order linear differential equations [13]. Here, we focus on the time-independent or infinite-horizon variation of LQR. In state space representation, the system must be representable by (2)

$$\dot{x} = \mathrm{A}x + \mathrm{B}u \tag{2}$$

where x is an Nx1 vector of state variables and A and B are NxN positive semi-definite non-singular matrices. The solution optimizes control for a cost functional defined by (3)

$$J(t) = \frac{1}{2}\int_{t_0}^{t_f} x^T Q x + \ u^T R u \, dt \tag{3}$$

where Q is the NxN positive definite state-error cost matrix and R is the NxN positive definite input cost matrix. The control input vector u is calculated by solving the algebraic Riccati equation (4) for K and then solving for u by (5). MATLAB includes both the *care()* and *dare()* functions to solve the continuous and discrete-time algebraic Riccati equations.

$$\dot{K} = 0 = -KA \ - \ A^T K \ - Q + KBR^{-1}B^T K \tag{4}$$

$$u = -R^{-1}B^T K X \tag{5}$$

As long as the system as stabilizable, the control input u will always yield a stable system (negative real part of eigenvalues). However this method has convergence issues when computation time steps are too large. The Riccati solvers also have convergence issues if the A, B, Q, or R matrices are singular or ill-conditioned.

B. Linearization and State-Space Representation

Since CPL impedance varies non-linearly both from loading and bus voltage, the system matrix A is variable and non-linear. To develop the A matrix for use in LQR, we must first linearize the differential equations of (1) about the instantaneous CPL terminal voltage and power. The CPL small-signal linear resistance is found by first estimating CPL load by summing currents in (6) and combining that information with the instantaneous CPL voltage in (7). From there, the linearized A matrix can be formed for use by the Riccati equation (5).

$$P_{CPL_x} = \ Vb_x * \left(Ib_x - \ Cb_x \frac{d}{dt} Vb_x + Is_x\right) \tag{6}$$

$$R_{CPL} = \frac{dV}{dI} = \frac{d}{dI} V_{CPL} = \frac{d}{dI} * \frac{P_{CPL}}{I} = \ -\frac{P_{CPL}}{{I_{CPL}}^2} = \ -\frac{{Vb_x}^2}{P_{CPL}} \tag{7}$$

To implement the LQR routine, the state variables are defined so that steady-state values are zero. A level shift of all of the system values which will not be zero in steady-state creates the state-variable vector 'X'.

$$\begin{aligned}
X_1 &= \ Ig_1 - \ .80 * I0 \\
X_2 &= \ Ig_2 - \ .20 * I0 \\
X_3 &= \ V_{bus} - \ V_{ref} \\
X_4 &= \ Iz_1 - \ Io1 \\
X_5 &= \ Iz_2 - \ Io2 \\
X_6 &= \ Vz_1 - \ V_{ref} - \ Rz_1 * Io1 \\
X_7 &= \ Vz_2 - \ V_{ref} - \ Rz_2 * Io2 \\
X_8 &= \ Vd_1 - \ V_{ref} - \ Rz_1 * Io1 \\
X_9 &= \ Vd_2 - \ V_{ref} - \ Rz_2 * Io2 \\
X_{10} &= Ib_1 - Iob1 \\
X_{11} &= \ Ib_2 - \ Iob2 \\
X_{12} &= \ Vb_1 - \ V_{ref1} \\
X_{13} &= \ Vb_2 - \ V_{ref2}
\end{aligned} \tag{8}$$

where:
I0 is the steady state total MVDC current.
V_{ref} is the MVDC bus reference voltage (12kV).
Io1 is the zone #1 steady state MVDC current (P_{CPL1}/V_{ref}).
Io2 is the zone #2 steady state MVDC current (P_{CPL2}/V_{ref}).
Iob1 is the zone #1 steady state LVDC current (P_{CPL1}/V_{ref1}).
Iob2 is the zone #2 steady state LVDC current (P_{CPL2}/V_{ref2}).
V_{ref1} is the zone #1 LVDC reference voltage (1kV).
V_{ref2} is the zone #2 LVDC reference voltage (6kV).

Load sharing between PGMs is enforced by choosing the steady-state PGM currents to be 80% and 20% of total load current for PGM#1 and PGM#2 respectively.

While Q and R need only be positive definite, the number of values considered in design are minimized by choosing diagonal matrices for Q and R. The Q and R matrix diagonals are iteratively adjusted until results are satisfactory. Results were considered satisfactory when transient voltages remained within 10% of nominal values during the test transient.

C. *LQR-P Implementation*

Using the multi-rate LQR technique developed in [14], we first convert the continuous time differential equations of (1) into a discrete time difference equations, then we construct the periodic analogs to the A, B, Q, and R matrices.

Since the system under study has two switching cycles: one at 1kHz and another at 8kHz, we may define a super cycle of T_1 = 1ms which is subdivided into eight subcycles of T_2 = 0.125ms. Using the subcycle as a base unit of time, we must dicretize the contuous-time differential equations of (1) into discrete-time difference equations. This is easily accomplished by the transformation of equation (9) using T_2 as *dt*.

$$x(t + dt) \ = \ x(t) \ + \ \dot{x}(t) * dt \tag{9.a}$$

$$x[k+1] = x[k] + [Ax(t) + Bu(t)]dt \tag{9.b}$$

$$x[k+1] = (I + A * dt)x[k] + (B * dt)u[k] \tag{9.c}$$

$$x[k+1] = Fx[k] + Gu[k] \tag{9.d}$$

F and G matrices are constructed for each subcycle in our periodic system. In our case, F_1 through F_8 will be identical, as the state matrix does not change. G_1 will be for the subcycle where PGM#1 and both HESSs are switching, G_4 will be for the subcycle where PGM#2 and both HESSs are switching and all other G_x will be subcycles where only the two HESSs are switching. Since there is no reason to do otherwise, we maintain Q and R uniform through all eight subcycles. The periodic, or super cycle, A, B, Q, and R matrices are shown in (10). Once A, B, Q, and R are set, the discrete-time Riccati equation can be solved with the MATLAB *dare()* function, yielding the super cycle solution matrix K (11). The subcycle K_x can then be inserted into (5) using the corresponding subcycle R_x and G_x for R and B respectively.

$$A = \begin{bmatrix} 0 & F_8 & 0 & \dots & 0 \\ 0 & 0 & F_7 & \dots & 0 \\ \vdots & \vdots & \vdots & \ddots & \vdots \\ 0 & 0 & 0 & \cdots & F_2 \\ F_1 & 0 & 0 & \cdots & 0 \end{bmatrix} \quad B = \begin{bmatrix} 0 & G_8 & 0 & \dots & 0 \\ 0 & 0 & G_7 & \dots & 0 \\ \vdots & \vdots & \vdots & \ddots & \vdots \\ 0 & 0 & 0 & \cdots & G_2 \\ G_1 & 0 & 0 & \cdots & 0 \end{bmatrix}$$

$$Q = \begin{bmatrix} Q_1 & 0 & 0 & \dots & 0 \\ 0 & Q_8 & 0 & \dots & 0 \\ 0 & 0 & Q_7 & \dots & 0 \\ \vdots & \vdots & \vdots & \ddots & \vdots \\ 0 & 0 & 0 & \cdots & Q_2 \end{bmatrix} \quad R = \begin{bmatrix} R_1 & 0 & 0 & \dots & 0 \\ 0 & R_8 & 0 & \dots & 0 \\ 0 & 0 & R_7 & \dots & 0 \\ \vdots & \vdots & \vdots & \ddots & \vdots \\ 0 & 0 & 0 & \cdots & R_2 \end{bmatrix} \quad (10)$$

$$K = \begin{bmatrix} K_1 & 0 & 0 & \dots & 0 \\ 0 & K_8 & 0 & \dots & 0 \\ 0 & 0 & K_7 & \dots & 0 \\ \vdots & \vdots & \vdots & \ddots & \vdots \\ 0 & 0 & 0 & \cdots & K_2 \end{bmatrix} \quad (11)$$

In summary, the first step is to linearize the differential equations of (1), discretize the continuous-time state matrices into discrete-time state matrices (9), construct the supercycle A, B, Q, and R matrices(10), solve the discrete-time Riccati equation with MATLAB *dare()*to find K (11), then use the appropriate subcycle K_x to compute u (5) for the subcycle. Once u is calculated, updating the PGM voltages and HESS currents is straightforward. For cycles where PGM voltage is updated, the commanded PGM voltage is shown in (12) and (13). The commanded HESS current is shown in (14). Equations (12) and (13) include the u control term appropriate to the associated PGM as well as terms for the equilibrium voltage of the PGM.

$$E_{1_{new}} = u_{E1} + V_{ref} + Rg_1 * 0.80 * I0 \quad (12)$$

$$E_{2_{new}} = u_{E2} + V_{ref} + Rg_2 * 0.20 * I0 \quad (13)$$

$$Is_{new} = u_{Is} \quad (14)$$

D. LQR-SM Implementation

Here, we reiterate the selective input-cost matrix LQR-SM description that appears in [15]. Similar to the LQR-P implementation, we recognize that during one supercycle (PGM switching cycle) there are eight smaller subcycles (HESS switching cycles). One subcycle has PGM#1 switching simultaneously with both HESSs, another subcycle has PGM#2 switching simultaneously with both HESSs, while the remaining six subcycles have only the two HESSs inputs switching. Rather than develop the different B or G matrices as LQR-P does, we develop three different R matrices. To realize these three different R matrices for the three subcycles, we simply place a large R-penalty on the PGM(s) which are not being switched. An R-penalty value of 2-3 orders of magnitude greater than the values for active inputs is sufficient to nullify the input. In this way, we constrain the Riccati solver to maximize use of the available devices while minimizing input from the unavailable devices and thus mimic the true system. For example, during cycles where a PGM is being switched, its associated R-value from Table 2 is 15, but during subcycles where that PGM is not switching, the R-value is 10^3.

Unlike LQR-P, LQR-SM linearizes every subcycle. Once the differential equations of (1) are linearized, the appropriate R matrix for the subcycle is selected. Then, the continuous-time Riccati equation is solved for K using MATLAB *care()* and input vector u calculated by (5).

Once the PGM and HESS values have been calculated by (12)-(14), the DC-DC converter switching duty cycles for each device can be updated. The full LQR-SM computation cycle is illustrated in Fig. 4.

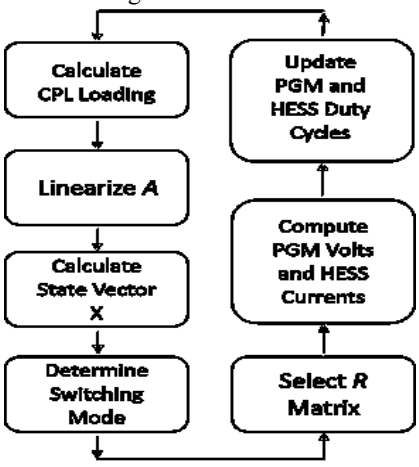

Figure 4 – Multi-rate Computation Cycle

IV. SIMULATION AND RESULTS

The simulations presented are for the average value model of a shipboard MVDC distribution system described in Fig. 3. The MVDC main bus voltage is 12kV while the two buck zones are 1kV and 6kV respectively. It is assumed that PGM inputs may be switched at a rate of 1kHz and HESS current may be switched at a rate of 8kHz. PGM voltage switching events occur on alternating half-cycles such that the two PGMs are never switched simultaneously. At time zero, CPL power is instantaneously stepped from 15 MW in zone #1 and 9 MW in zone #2 (total of 24 MW) to 20 MW in zone #1 and 28 MW in zone #2 (total of 48 MW). Power levels then return to their original values 20ms later. This is a step from 50% power to 100% power back to 50% power. The Q and R matrices were iteratively tuned to maintain peak voltage within 10% of reference values. Component values are shown

in Table 1. *Q* and *R* matrices for both LQR-P and LQR-SM trials are identical with values recorded in Table 2.

Table 1 – Component Values

Rg1	0.25 Ω	Lz1	70.5 µH	Cd1	1.7 µF
Rg2	0.30 Ω	Lz2	47.0 µH	Cd2	2.3 µF
Lg1	2.00 mH	Cz1	2.46 µF	Lb1	30.6 µH
Lg2	1.80 mH	Cz2	3.69 µF	Lb2	926 µH
Cbus	4.0 µF	Rd1	10 Ω	Cb1	75 mF
Rz1	3.30 mΩ	Rd2	10 Ω	Cb2	1.25 mF
Rz2	2.20 mΩ				

Table 2 – Cost Matrix Diagonals

Q	1	1	8	1	1	1	1	1	1	1	1	1176	42
R	15	15	$R_{3,3}.R_{11,11} = 10^3$									0.4	0.5

The simulation results demonstrate successful use of both LQR-P and LQR-SM to control and stabilize a large transient on an MVDC bus utilizing both PGM voltages and HESS currents as control inputs. Fig. 5a shows that PGM voltages vary more widely for LQR-P than for LQR-SM. Despite the greater differences in PGM voltages, the PGM currents in both LQR-P and LQR-SM cases are very similar, illustrated in Fig. 5b. We especially see that the larger machine, PGM#1, currents match more closely than for the smaller machine, PGM#2. This appears to be due to the larger differences between the PGM#2 voltages commanded by LQR-P versus LQR-SM. Also noticeable is that the LQR-SM PGM voltages reach steady-state values after only 5ms while the LQR-P PGM voltages require about 15ms to reach steady-state values.

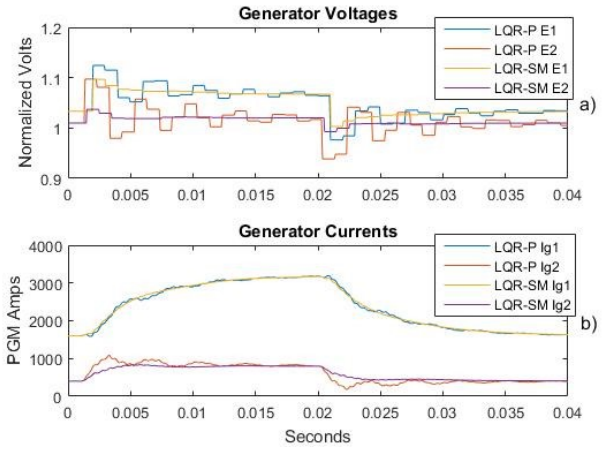

Figure 5 – PGM Performance

In Fig. 6, we see that MVDC bus voltage varies by up to 8% from nominal voltage in the LQR-P case, but only 3% for LQR-SM. This difference appears to be due to LQR-SM having lower variation and quicker settling time for PGM voltage.

Fig. 7a illustrates the normalized voltages in the low-voltage buses supplied by the buck converters. Results for LQR-P and LQR-SM are not identical, but have very similar overshoot and settling time values. LQR-P appears to have slightly more overshoot, but a slightly quicker settling time in Zone#1. In Zone#2, LQR-P has slightly less overshoot, but settling times are near identical. In Zone#2 we also see that LQR-P voltage has a high-frequency component not visible in the LQR-SM result. This high-frequency "wiggle" is most likely the result of the wider PGM voltage swings that produced the large MVDC bus voltage disturbances. Examining Fig. 7b, we see only small differences between the LQR-P and LQR-SM results.

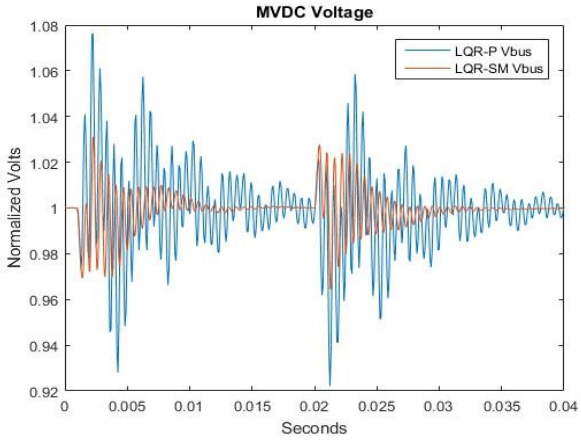

Figure 6 – Main MVDC Bus Voltage

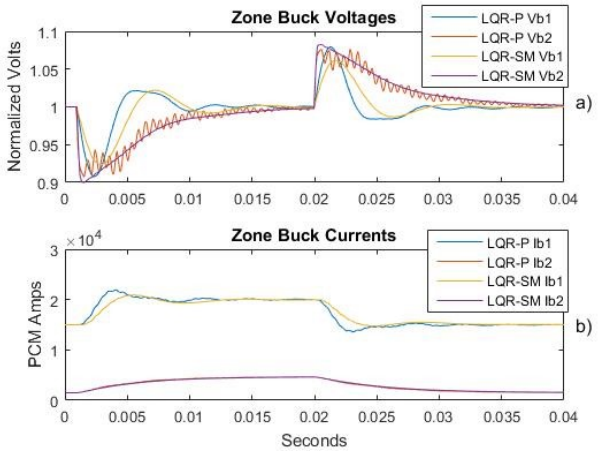

Figure 7 – Zone Normalized Volts and Currents from Buck Converters

Examining the power and energy delivered by the HESSs in both the LQR-P and LQR-SM cases, again the results are very similar. In Fig. 8a especially we see that in Zone#2 the HESS power fluctuates much greater in the LQR-P case than in the LQR-SM case. This is due to the HESS acting to overcome the MVDC bus voltage fluctuations described earlier. Looking at Fig. 8b, however we see that the LQR-P case requires less energy to stabilize the transient than the LQR-SM case. This is true in both Zone#1 and Zone#2.

Here we should also mention computational complexity. LQR-P constructs supercycle matrices that are the number of

subscycles squared larger than the matrices developed by LQR-SM. In this example, LQR-P supercycle matrices are 104x104 while the LQR-SM matrices are only 13x13. LQR-P only requires the Riccati equation to be solved once per supercycle whereas LQR-SM solves the Riccati equation every subcycle; however, the vastly larger size of LQR-P supercycle matrices still demands greater computing power. To illustrate, the LQR-P simulation shown took roughly 28 seconds for MATLAB to run, while the LQR-SM simulation took about 2 seconds.

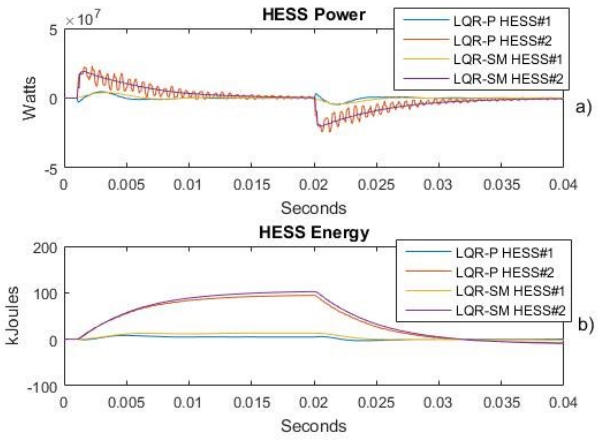

Figure 8 – HESS Power and Delivered Energy

V. Conclusion

In this paper two different implementations of adaptive, multi-rate LQR were presented as potential control schemes to ensure stable operation of a hypothetical MVDC shipboard power system with instantaneously stepped constant power loads. Both control schemes provided exemplary MVDC and zone bus regulation by coordinating the use of PGM voltages and HESS currents. The provided example MVDC shipboard power system illustrates the value of a true multi-input control scheme for use in systems which may not be simplified into low-order systems of a single source and an ideal constant power load.

The first control scheme implemented, LQR-P, provides robust control. For a given set of *Q* and *R* cost matrices, LQR-P is demonstrated to have greater high-frequency oscillations among input devices compared to LQR-SM, resulting in longer settling time and poorer MVDC bus regulation. Conversely, LQR-P appears to have lower overshoot levels and requires less HESS energy to stabilize the transient. With lower HESS utilization to achieve similar results, the LQR-P stabilized system may allow the use of smaller HESSs. A negative attribute of the LQR-P control scheme is that it is much more computationally expensive than LQR-SM.

LQR-SM produces nearly identical results to LQR-P when both control methods utilize the same *Q* and *R* matrices. When controlled by LQR-SM the test model had a faster settling time and superior MVDC bus regulation (3% vs 8% for LQR-P). Under these same conditions, LQR-SM control requires more stabilizing energy from the HESSs than LQR-P. The greatest advantage of LQR-SM over LQR-P is a much lower computation requirement. With more extensive tuning of the Q and R matrices, the performance differences between the two methods may be eliminated; but the computational advantage of LQR-SM will remain.

VI. References

[1] John Kusean, "Naval Power Systems Technology Development Roadmap", Naval Sea Systems Command PMS 320, April 2013.

[2] Norbert Doerry, John Amy, and Cy Krolick "History and Status of Electric Ship Propulsion, Integrated Power Systems, and Future Trends in the U.S. Navy," Proceedings of the IEEE, Vol. 103, No.12, December 2015, pp2243-2251.

[3] C.G. Hodge, J.O. Flower and A. Macalinden, "DC Power System Stability," *IEEE Electric Ship Technologies Symposium*, pp433-439, 2009.

[4] Alexis Kwasinski and Chimaobi N. Onwucheckwa, "Dynamic Behavior and Stabilization of DC Microgrids with Instantaneous Constant power Loads," IEEE Transactions on Power Electronics, Vol. 26, No. 3, March 2011, pp822-834.

[5] Maria Stefania Carmeli; Denis Forlani; Samuele Grillo; Roberto Pinetti; Enrico Ragaini; Enrico Tironi , "A Stabilization Method for DC Networks with Constant-Power Loads," *IEEE International Energy Conference and Exhibition (ENERGYCON),* pp617 – 622, 2012.

[6] Luis Herrera, Wei Zhang, Jin Wang, "Stability Analysis and Controller Design of DC Microgrids with Constant Power Loads," IEEE Transactions on Smart Grid, Vol. 8, No. 2, March, pp881-888, 2017

[7] Qianwen Xu, Xiaolei Hu, etc, "Design and Stability Analysis for an Autonomous DC Microgrid with Constant Power Loads," IEEE Applied Power Electronics Conference and Exposition, pp3409-3415, 2016.

[8] Vittorio Arcidiacono; Antonello Monti; Giorgio Sulligoi, "An Innovative Generation Control System for Improving Design and Stability of Shipboard Medium-Voltage DC Integrated Power System," *IEEE Electric Ship Technologies Symposium,* pp152 – 156, 2009.

[9] Giorgio Sulligoi; Daniele Bosich; Lin Zhu; Marco Cupelli; Antonello Monti, "Linearizing Control of Shipboard Multi-Machine MVDC Power Systems Feeding Constant Power Loads," IEEE Energy *Conversion Congress and Exposition (ECCE),* pp691 – 697, 2012.

[10] Sulligoi, G., D. Bosich, G. Giadrossi, L. Zhu, M. Cupelli, A. Monti, "Multiconverter Medium Voltage DC Power Systems on Ships: Constant-Power Loads Instability Solution Using Linearization via State-Feedback Control," *IEEE Transactions on Smart Grid*, Vol 5, No 5, September, pp2543-2552, 2014.

[11] Marco Cupelli; Markus Mirz; Antonello Monti, "Application of Backstepping to MVDC Ship Power Systems with Constant Power Loads," *International Conference on Electrical Systems for Aircraft, Railway, Ship Propulsion and Road Vehicles (ESARS),* pp1 – 6, 2015 .

[12] Lin Zhu; Junqi Liu; Marco Cupelli; Antonello Monti, "Decentralized Linear Quadratic Gaussian Control of Multi-Generator MVDC Shipboard Power System with Constant Power Loads," IEEE Electric Ship Technologies Symposium (ESTS), pp308 – 313, 2013.

[13] Kirk, Donald E., "Optimal Control Theory: An introduction," Dover Publications Inc, Mineola NY, 1998.

[14] K. Natarajan and R. Balasubrumanian, "One the Design of LQR Multirate Controllers," IEEE American Control Conference, pp1974-1979, 1986.

[15] Adam Mills and Robert Ashton, "Adaptive, Sparse, and Multi-rate LQR Control of an MVDC Shipboard Power System with Constant Power Loads," IEEE International Conference on Industrial Technology 2017, publication pending.